Received: 15 March 2021 | Revised: 1 April 2022 | Accepted: 19 April 2022 | Published on: 31 May 2022

DOI: 10.1002/qj.4295

Quarterly Journal of the Royal Meteorological Society RMetS

RESEARCH ARTICLE

Combined effects of soil moisture and microphysical perturbations on convective clouds and precipitation for a locally forced case over Central Europe

Florian Baur[1,2] | **Christian Keil**[1] | **Christian Barthlott**[3]

[1]Meteorologisches Institut, Ludwig-Maximilians-Universität, Munich, Germany

[2]Deutscher Wetterdienst, Offenbach am Main, Germany

[3]Institute of Meteorology and Climate Research (IMK–TRO), Karlsruhe Institute of Technology (KIT), Karlsruhe, Germany

Correspondence
Florian Baur, Meteorologisches Institut, Ludwig-Maximilians-Universität, Munich 80333, Germany.
Email: Florian.Baur@lmu.de

Funding information
This work was supported by the Deutscher Wetterdienst research program Innovation Programme for applied Researches and Developments (IAFE). This research has been performed within project B3 of the Transregional Collaborative Research Center SFB/TRR 165 "Waves to Weather" funded by the German Research Foundation (DFG). The authors wish to thank the Deutscher Wetterdienst (DWD) for providing the COSMO model code, analyses and radar-derived precipitation data.

Abstract

To study the combined impact of soil moisture and microphysical perturbations on convective clouds and precipitation over Central Europe, an ensemble of five dozen real-world weather prediction forecasts was conducted with the COnsortium for Small-scale MOdeling (COSMO) model at convection-permitting resolution for a case with weak large-scale forcing (6 June 2016). We find a large sensitivity of precipitation, ranging from +10% to −23% in 12-hr precipitation totals. While the homogeneous soil-moisture bias of ±25% primarily controls the timing of convection initiation and the amount of surface rainfall, the number of cloud condensation nuclei and width of the cloud droplet size distribution mainly control the number, size, and lifetime of convective clouds. In moisture-limited conditions, mainly positive couplings are acting. Drier soils, cleaner air, and a broader cloud droplet size distribution result in less rainfall. Wetter soils and more polluted conditions lead to fewer, but larger, cloud clusters. Since microphysical process rates depend systematically on the sign of the perturbations, but rainfall does not, there are compensating effects at work that buffer microphysical perturbations directly and impact the cloud condensate amount and the rainfall at the ground.

KEYWORDS

cloud condensation nuclei, cloud droplet size distribution, convective precipitation, microphysical process rates, precipitation efficiency, rain formation processes, soil moisture

1 | INTRODUCTION

Despite improvements in the parametrizations of physical processes and higher resolution of numerical weather prediction (NWP) models over the past decades, the successful forecasting of cloud formation and convective precipitation still remains a challenge for convective-scale NWP models. As convective processes are increasingly resolved in these models, other sources of uncertainty, like, for example, land–atmosphere interactions and cloud microphysics, become more relevant. Land-surface properties (e.g., land cover, terrain, and soil texture) are highly heterogeneous across a wide range of scales, and potential linkages between land-surface variables

and atmospheric variables such as temperature and precipitation are difficult to establish (e.g., Seneviratne *et al.*, 2010; Kirshbaum *et al.*, 2018). With prevailing weak synoptic-scale forcing, land–atmosphere interactions are assumed to be decisive for cloud formation and the subsequent convective precipitation. The effect of soil-moisture anomalies on the formation of precipitation in the mid-latitudes using convective-scale NWP models in real case scenarios has rarely been examined so far. Hohenegger *et al.* (2009) and Barthlott *et al.* (2011) showed a strong case dependence of the soil-moisture–precipitation coupling. The decisive role of the prevailing weather regime on the sign of coupling of soil-moisture perturbations and convective afternoon precipitation was shown by Baur *et al.* (2018). Averaged over seven synoptically weakly forced cases, they found a positive coupling between the overall soil-moisture bias and the domain-averaged precipitation.

A further source of uncertainty in convective-scale modelling arises from the nonlinear character of the microphysics and the complexity of the microphysical system, with many possible process pathways (e.g., Seifert *et al.*, 2012). Aerosol–cloud interactions are among the most uncertain processes in NWP models, and the large variability of cloud physics parametrizations results in a large spread of modelling results (e.g., Fan *et al.*, 2016). Recently, Glassmeier and Lohmann (2018) studied the sensitivity of warm- and mixed-phase orographic precipitation to aerosol backgrounds with idealized 2D simulations. They found that the precipitation response to aerosol perturbations is buffered, compared with the response of cloud variables. Recent work also documented that the effect of aerosols on cloud formation and subsequent precipitation varies in sign and magnitude for different situations. For example, using idealized simulations, Grant and van den Heever (2015) showed that aerosol effects on deep convective clouds are also modulated by the altitude of dry layers and that the aerosol impacts vary inversely with storm organization. Realistic simulations for six cases with different weather regimes were investigated by Barthlott and Hoose (2018). They found a systematic decrease of total precipitation with increasing cloud condensation nuclei (CCN) concentrations for cases with strong synoptic forcing caused by a suppressed warm-rain process, whereas no systematic aerosol effect is simulated for weak synoptic forcing.

In addition, the width of the cloud droplet size distribution (CDSD), which is controlled by the shape parameter ν, has important implications for microphysical processes and cloud characteristics. Using large-eddy simulations of nonprecipitating shallow cumulus clouds, Igel and van den Heever (2017b) have shown that the evaporation rates are much more sensitive to the value of the shape parameter than to the condensation rates. As a result, cloud properties such as droplet number concentration, mean droplet diameter, and cloud fraction are strongly impacted by the value of the shape parameter. The changes were found to be of the same order of magnitude as changes due to increasing or decreasing the aerosol concentration by a factor of 16. Furthermore, the cloud albedo increased with higher values of the shape parameter, which also has important implications for cloud characteristics and development. As there is a large range in shape parameter values based on cloud type and environmental conditions (Morrison and Grabowski, 2007; Igel and van den Heever, 2017b), it constitutes a parameter well suited to studying microphysical uncertainty. Barthlott *et al.* (2022) have found that a smaller width of CDSD can produce almost as large a variation in precipitation as a CCN increase from maritime to polluted conditions. Modifications of the shape parameter affect several processes, such as evaporation, water-vapour deposition, radiation, and heating rates. The inclusion of microphysical uncertainties by perturbing CDSD parameters in convective-scale models is therefore very promising.

While the individual driving processes for convection initiation and cloud development have been studied extensively in recent years, only a few researchers have investigated their combined effects. Imamovic *et al.* (2017) conducted convection-resolving simulations with a simplified land surface to dissect the isolated and combined impacts of soil moisture and orography on deep convective precipitation for an initial profile corresponding to typical European summer climate conditions. They found a consistently positive soil-moisture–precipitation feedback for horizontally uniform perturbations, irrespective of the presence of low orography. However, a negative feedback with localized perturbations emerged. A dry soil heterogeneity enhances rain amounts, which scale linearly with the dryness of the soil, while a moist heterogeneity suppresses rain amounts. Schneider *et al.* (2019) investigated the relative impact of soil moisture and aerosols combined with orographic effects. They performed simulations with the COnsortium for Small-scale MOdeling (COSMO) model with 500 m grid length for six real-case events over Germany, with systematic changes in the initial soil-moisture fields and different assumptions about the ambient aerosol concentration. The model produced a positive soil-moisture–precipitation feedback for most of the cases, with the soil moisture amount having a stronger effect on precipitation than on its spatial distribution. The precipitation response to changes in the CCN concentration was found to be more complex and case-dependent. However, both aerosols and soil-moisture uncertainties were of similar importance for quantitative precipitation forecasting.

The goal of this study is to estimate quantitatively the impact of different sources of uncertainty by investigating the combined effect of soil moisture and microphysical uncertainties, such as CCN concentration and CDSD, in order to understand better the mechanisms for cloud formation and subsequent precipitation for a well-studied single case study during weak synoptic control. The concept of combined perturbations (instead of perturbing one parameter alone) is especially challenging and gives additional insight into the role of different uncertainties and how they affect convective precipitation. This work is embedded in numerous articles (Baur *et al.*, 2018; Rasp *et al.*, 2018; Zeng *et al.*, 2018; Hirt *et al.*, 2019; Keil *et al.*, 2019) addressing different aspects of predictability that focus on a 10-day high-impact weather period characterized by frequent heavy precipitation events across Central Europe in early summer 2016. On four out of these ten days, weather was determined by weak synoptic control, characterized by a clear diurnal cycle of convection triggered by local processes not disturbed by transient synoptic weather systems. Several studies (e.g., Barthlott and Hoose, 2018; Baur *et al.*, 2018; Keil *et al.*, 2019) showed that the atmosphere reacts more sensitively to soil-moisture perturbations and various aerosol concentrations during weak synoptic forcing. Hence, we herein constrain the numerical experimentation to a single weather situation with a potentially larger than average impact on clouds and rainfall. The case of 6 June 2016 has been selected as a typical atmospheric scenario governed by weak synoptic control and serves as a prototype for studying the collective influence. We intentionally disregard the key sources of uncertainty in limited-area modelling (initial conditions, lateral boundary conditions, model error) and focus exclusively on the joint impact of the three perturbations on microphysical process rates, the ensuing clouds, and ultimately surface precipitation. The novel aspect of this work is the fact that soil moisture and microphysical uncertainties are combined in realistic convection-resolving simulations. Although only one case study is examined here, this study represents another piece in the mosaic required to elaborate on the perturbation strategy in convective-scale models in order to describe convective-scale predictability adequately, and can be considered as a proof-of-concept to assess the possible value of combined sensitivities.

2 | METHODOLOGY

2.1 | Model description

All numerical experiments are performed with the convective-scale COSMO model (until February 2021 the operational forecast model of the Consortium for Small-Scale MOdeling, version 5.05: Schättler *et al.*, 2018). The model covers Germany and parts of the neighbouring countries, including most of the Alps (Figure 1a). This domain is covered using a spatial resolution of 0.025 ° in the horizontal, resulting in 461 by 421 grid cells with an approximate spacing of 2.8 km, 50 vertical levels, and a time step of 25 s. The evaluation is performed for a subdomain largely covering Germany (depicted by the grey box in Figure 1a). All experiments are initialized at 0000 UTC, driven by hourly COSMO-EU analyses (i.e., the operational 7-km model version covering the whole of Europe). Similar to Barthlott and Hoose (2018) and in contrast to the model setup used operationally, we applied a two-moment microphysics scheme (Seifert and Beheng, 2006). This microphysics scheme calculates both mass mixing ratios and number concentrations of various hydrometeors, including rain, hail, graupel, and snow. The activation of CCN from aerosol particles is based on precalculated activation ratios stored in lookup tables (Segal

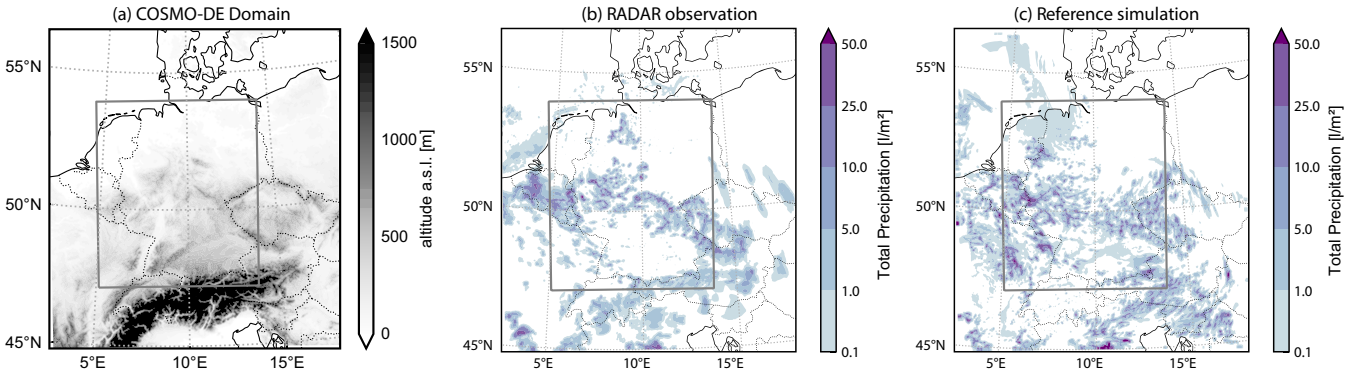

FIGURE 1 (a) COSMO-DE domain with the investigation region (inner frame). Also shown are the orography in greyscale, political boundaries as dotted lines, and coastlines as black solid lines. Daily accumulated precipitation (b) derived from RADAR observations (RADOLAN) and (c) of the reference simulation (*B100*; $\nu = 0$; CCN = 1700 cm^{-3}), valid on 6 June, 2016 [Colour figure can be viewed at wileyonlinelibrary.com]

and Khain, 2006), which depend on the properties of the aerosol and the vertical velocity at cloud base.

2.2 | Perturbation strategy

Firstly, the moisture content of the soil is perturbed by imposing a uniform soil-moisture bias. For that purpose, we increase/reduce (moist bias *B125*/dry bias *B075*) the initial soil-moisture content by 25% relative to the reference state (*B100*). The bias of ±25% is motivated by Hauck *et al.* (2011). They found that the mean bias between soil-moisture measurements and the COSMO state ranges between 20% and 30% in the southwestern region of the modelling domain.

Secondly, four different aerosol settings are prescribed in this study. These differ in the number density of condensation nuclei (N_{CN}), the mean radius of aerosols, and the aerosol mode standard deviation. The aerosol settings include *Maritime* ($N_{CN} = 100\ cm^{-3}$), *Intermediate* ($N_{CN} = 500\ cm^{-3}$), *Continental* ($N_{CN} = 1700\ cm^{-3}$), and *Continental Polluted* ($N_{CN} = 3200\ cm^{-3}$). The aerosol setting *Continental*, a typical setting for the Central European region, is used as the reference setting.

The third perturbed quantity represents the shape parameter ν of the cloud droplet size distribution (CDSD). This parameter mainly determines the width of the CDSD, as shown in Figure 2. In our experiments, we use five discrete values, $\nu = [0, 1, 2, 4, 8]$. The larger the shape parameter, the narrower the CDSD. Consequently, $\nu = 0$ represents the broadest CDSD, whereas $\nu = 8$ leads to the narrowest CDSD. This choice is similar to Igel and van den Heever (2017a) and represents a realistic range of values. This range was also investigated in idealized simulations by Wellmann *et al.* (2020). The reference value is chosen to be $\nu = 0$, which is the default value in the COSMO model. All combinations of perturbations add up to 60 COSMO experiments performed for a single real case study.

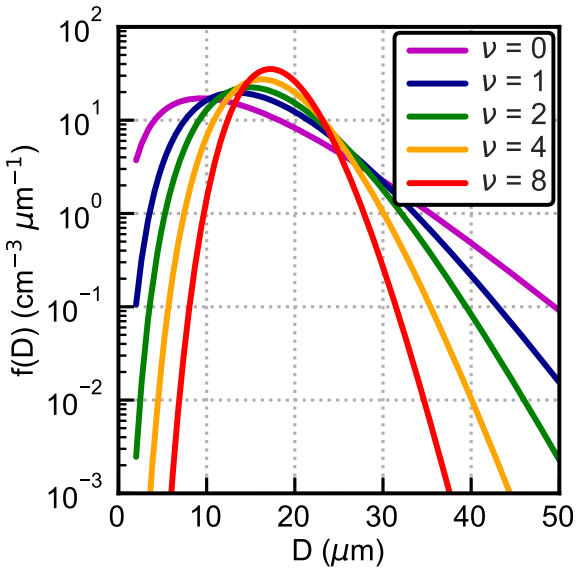

FIGURE 2 Example cloud droplet size distributions (DSD) with different shape parameters $\nu = [0, 1, 2, 4, 8]$. All graphs are calculated with a fixed number concentration of droplets ($300\ cm^{-3}$) and mixing ratio ($1.0\ g{\cdot}m^{-3}$) [Colour figure can be viewed at wileyonlinelibrary.com]

2.3 | Case study

We chose a synoptically weakly forced case, as the response is supposed to be stronger for soil-moisture perturbations (e.g., Baur *et al.*, 2018; Keil *et al.*, 2019) and microphysical changes (e.g., Barthlott and Hoose, 2018; Keil *et al.*, 2019). The meteorological conditions on 6 June, 2016 represent a characteristic case during the high-impact weather period in 2016 with daily recurring heavy precipitation over Central Europe (Piper *et al.*, 2016). The synoptic situation was characterized by two upper-level troughs forming a blocking situation over Central Europe and allowing for a persistent weak pressure gradient over the investigation area. This situation favoured low thermal stability and low mid-tropospheric wind speed, fostering intense moist convection with precipitation rates of more than $100\ mm{\cdot}hr^{-1}$. Figure 1b illustrates the typical precipitation fingerprint of such a weather situation, with a spotty, crumble-like spatial pattern. A comparison between the radar observations (Figure 1b) and the reference simulation (Figure 1c) shows that the COSMO model reproduces the weather situation reasonably well. The domain-averaged, hourly precipitation of the reference simulation (*B100*; $\nu = 0$; CCN = $1700\ cm^{-3}$) shows a characteristic diurnal cycle of convection with a pronounced peak in the afternoon (black curve in Figure 3).

3 | RESULTS

3.1 | Time series of precipitation rate and cloud water content

The case of 6 June 2016 represents a summer day with local convection spread over most of the domain, showing a characteristic diurnal cycle of convective precipitation attaining the strongest rainfall rates in the afternoon between 1400 and 1600 UTC (Figure 3). The most vigorous onset of convective precipitation is achieved by a reduction of soil moisture (−25%) and the narrowest CDSD (*B075*, $\nu = 8$, CCN = $1700\ cm^{-3}$; violet). This parameter combination leads to a more vigorous precipitation onset, leading

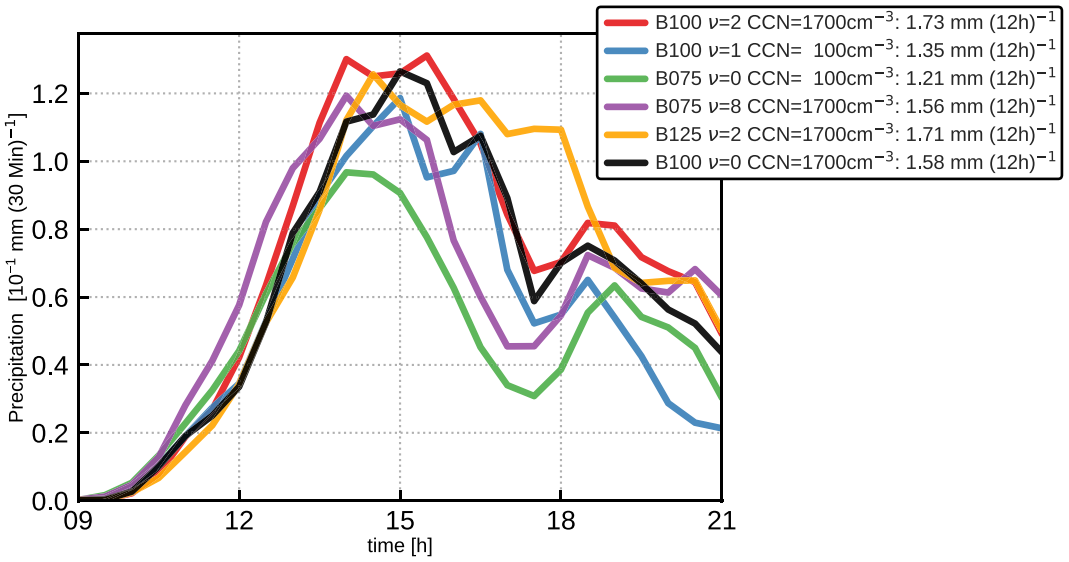

FIGURE 3 Time series of area-averaged, half-hourly precipitation evaluated for 6 June, 2016. The reference simulation (*B100*; $\nu = 0$; CCN = 1700 cm^{-3}) is displayed in black. Furthermore, the experiments with the highest precipitation amount (*B100*; $\nu = 2$; CCN = 1700 cm^{-3}, red), the lowest precipitation amount without perturbing the soil moisture (*B100*; $\nu = 1$; CCN = 100 cm^{-3}, blue), the overall lowest precipitation amount (*B075*; $\nu = 0$; CCN = 100 cm^{-3}, green), and the most vigorous onset of convective precipitation (*B075*; $\nu = 8$; CCN = 1700 cm^{-3}, violet) are shown [Colour figure can be viewed at wileyonlinelibrary.com]

to an increase in precipitation about 1 hr before the reference simulation (*B100*; $\nu = 0$; CCN = 1700 cm^{-3}; black). The increase in total 12-hr precipitation, however, only amounts to 1.4% compared with the reference simulation, due to limited moisture supply from the dry soil. The lowest precipitation (23% less than the reference) is produced with dry soils in combination with clean air, but keeping the reference broad CDSD (green curve in Figure 3). This is supported by a reduction in convective available potential energy (CAPE) by a factor of about 1/3 with lower initial soil moisture in the *B075* experiments (not shown). Interestingly, the largest increase in surface precipitation is not generated by wet soils combined with extreme microphysical perturbations, but occurs for an experiment in which only the shape parameter is modified (to a moderate value of $\nu = 2$), keeping initial soil moisture and CCN as in the reference. This combination leads to a precipitation increase of about 10% (red curve in Figure 3).

Figure 3 only shows a small subset of the 60 experiments, highlighting the full spectrum of possible scenarios comprising maximal or minimal precipitation for given soil-moisture initialization or the earliest onset. These selected experiments suggest a nonsystematic response of surface precipitation to the perturbations. In order to get an impression of the general influence of the different perturbation combinations, Figure 4 illustrates domain-averaged time series of (a,b) precipitation and (c,d) total column integrated cloud water for all experiments. Focusing on domain-averaged precipitation (panel a) reveals that the dry-bias simulations (*B075*, red) show the fastest increase in precipitation, whereas the moist-bias simulations (*B125*, blue) show the slowest. This leads to a negative soil-moisture–precipitation coupling during the initiation phase, resulting in an earlier onset of convection of the order of earlier by one hour. During the afternoon, the response of precipitation to soil-moisture perturbations is reversed. The highest precipitation rates are achieved by the moist-bias simulations, whereas the dry-bias experiments show the smallest rates. The simulations with reference soil moisture (green lines) always lie in between the perturbed soil-moisture configurations. This more rapid increase in precipitation in numerical simulations with a dry soil-moisture bias and a longer duration of precipitation in moist bias conditions has already been shown in earlier studies (Cioni and Hohenegger, 2017; Baur *et al.*, 2018). In general, the experiments sharing the same initial soil moisture agree well, as the precipitation deviations from the mean values of each group amount to about 3% only. While this behaviour leads to a grouping of the experiments according to the initial soil-moisture content, the different CCN concentrations do not show such a clear clustering focusing on precipitation (Figure 4b).

In contrast, the domain-averaged time series of total column-integrated cloud water (TQC) shows a different clustering (Figure 4c). Firstly, the dry-bias simulations lead to the quickest increase in TQC shortly after 0900 UTC, while the moist-bias experiments lead to the slowest increase, similar to surface precipitation. Contrary

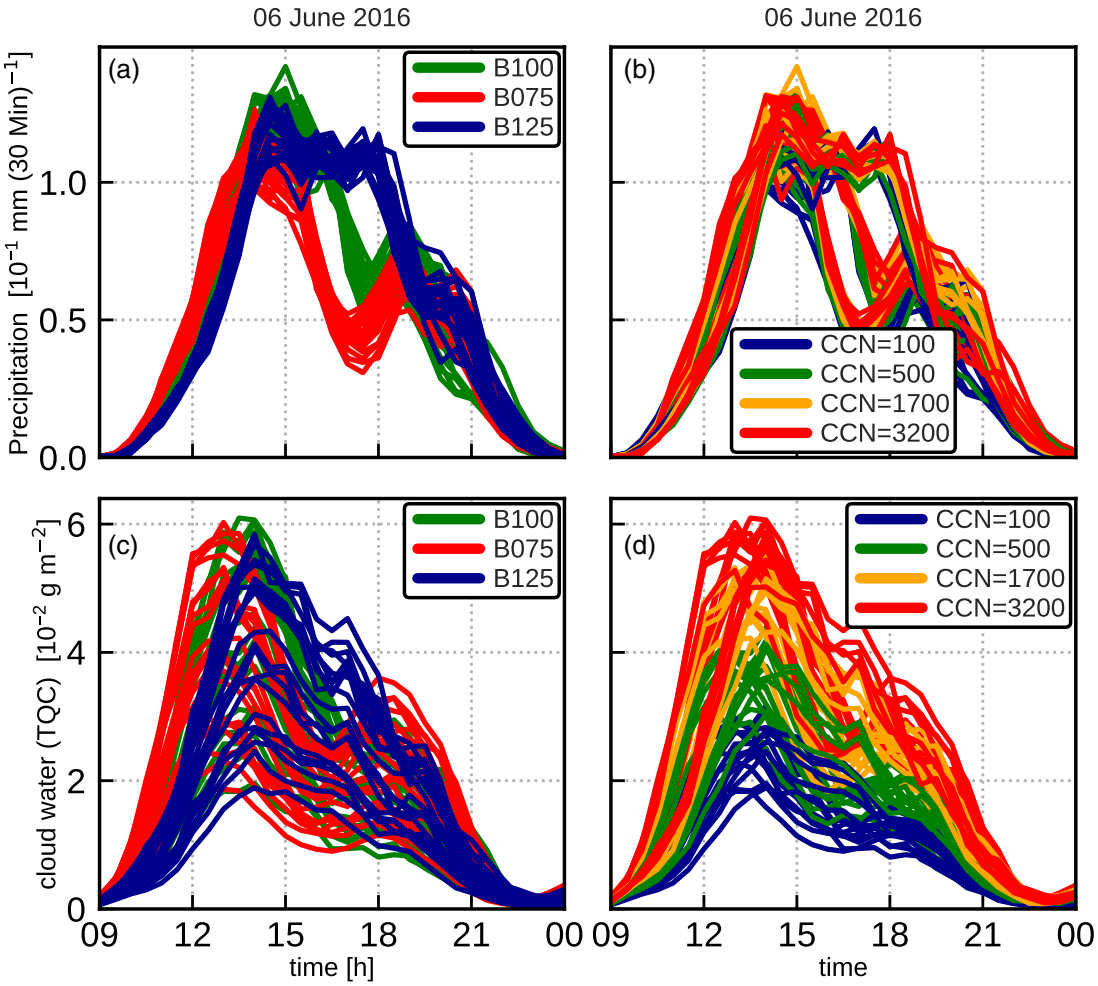

FIGURE 4 Time series of (a,b) domain-averaged half-hourly precipitation and (c,d) total column-integrated cloud water of all 60 experiments. Panels (a,c) are coloured according to the initial soil moisture, while panels (c,d) are coloured according to the CCN concentration [Colour figure can be viewed at wileyonlinelibrary.com]

to our intuition that TQC ought to behave similarly to surface precipitation, as it is a preceding quantity, initial soil moisture shows no systematic influence after precipitation onset. Instead, TQC sorts according to the CCN concentration (Figure 4d). High CCN concentrations (red) show the highest values of cloud water, whereas clean conditions (blue) show the lowest. This reflects the suppression of the warm-rain process in higher CCN regimes, which is also apparent in smaller autoconversion rates (see Section 3.3). Within each CCN group, there is a larger variability, with deviations of up to 25% from the respective mean TQC. This points towards a less uniform response of TQC to the CCN amount compared with the soil-moisture–precipitation coupling. Overall, soil-moisture perturbations control the precipitation, whereas the CCN concentration primarily governs the cloud water content. However, we have to consider the fact that changing the soil moisture also changes the thermodynamic environment in which clouds form. Soil moisture has a direct influence on the partitioning of the available energy at the ground into sensible and latent heat. As a consequence, boundary-layer temperature and moisture are affected, which usually increases CAPE for wetter soils, and the availability of water vapour to form clouds.

3.2 | Domain-averaged precipitation and cloud quantities

The time series shown in Figure 4 do not fully uncover a systematic impact of macro- and microphysical perturbations that would allow us to understand the different behaviour of precipitation and clouds. To focus more on the overall systematic linkage between perturbations and surface precipitation, we show area-integrated precipitation totals (accumulated between 0900 and 2100 UTC) of each experiment relative to the precipitation amount of the reference simulation (orange circles). The experiments are arranged in Figure 5 with increasing soil moisture

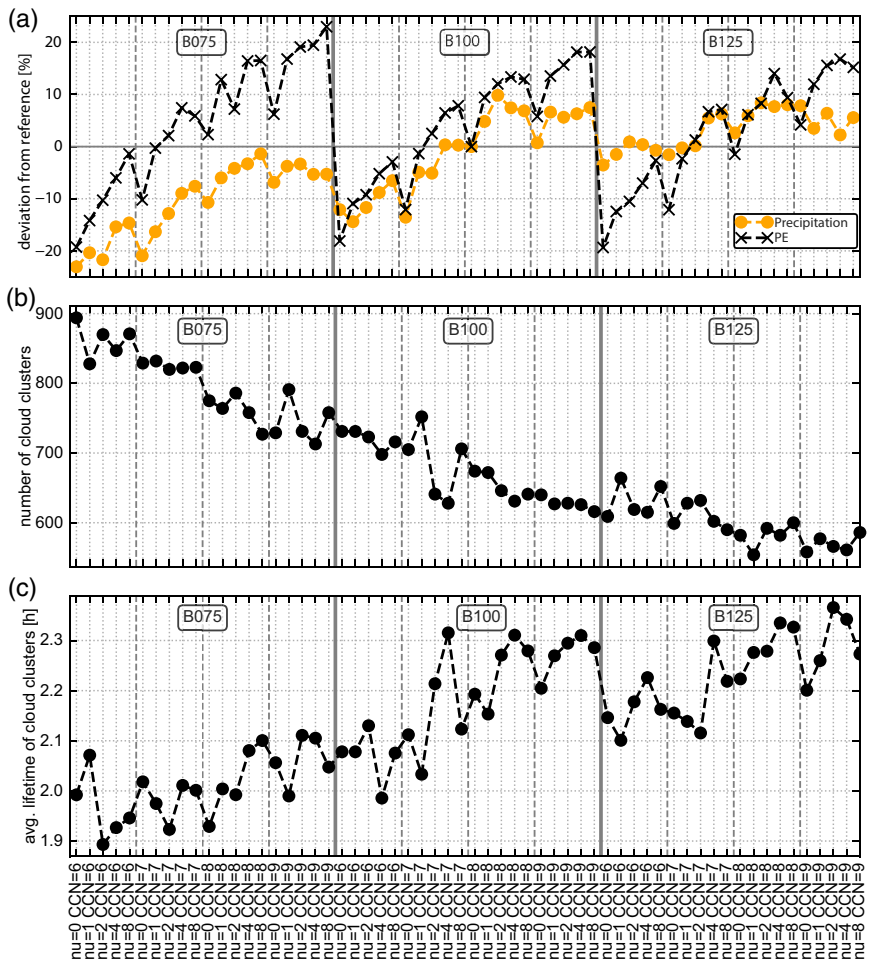

FIGURE 5 (a) Relative change (i.e., $(x - x_{ref})/x_{ref}$) in 12-hourly accumulated surface precipitation (orange circles) and 12-hourly relative change in precipitation efficiency (PE, equation 1; black crosses) relative to the reference experiment (SM=*B100*, $\nu = 0$, CCN = 1700 cm^{-3}). Precipitation efficiency is calculated for grid cells with precipitation exceeding 1.0 mm·hr^{-1} in the respective experiment. (b) Domain-averaged number of cloud clusters. (c) Average lifetime of cloud clusters (in hours). Evaluations are performed for a timeframe between 0900 and 2100 UTC and for every single experiment. Note that, for the sake of brevity, the different CCN concentrations are abbreviated by CCN = 6 (100 cm^{-3}), 7 (500 cm^{-3}), 8 (1700 cm^{-3}), and 9 (3200 cm^{-3}) [Colour figure can be viewed at wileyonlinelibrary.com]

(the dry bias experiments (*B075*) to the left, the bias-free experiments in the centre, and the moist-bias experiments (*B125*) to the right). Within each soil moisture group (e.g., *B075*), the experiments are sorted firstly according to the CCN concentration and secondly according to the shape parameter ν.

Dry soils (*B075* experiments) reduce precipitation totals, indicating a positive coupling. In comparison with the reference simulation, all dry bias experiments show a decrease in accumulated precipitation, ranging between −1% and −23%. For CCN concentrations less than 3200 cm^{-3}, precipitation increases systematically with higher CCN concentration. A closer look into the four CCN subgroups reveals accumulated precipitation to be secondarily sensitive to CDSD. Precipitation mostly increases with increasing shape parameter ν (i.e., narrower CDSD), leading to the sawtooth-like shape of the relative precipitation deviations in Figure 5a. Differences caused by the different shape parameters are in the range of 10%, with the lowest precipitation for small and highest precipitation for large shape parameters. This sawtooth-like increasing trend, however, is interrupted for the highest CCN concentration (3200 cm^{-3}).

A similar behaviour is discernible for the soil-moisture bias-free simulations. The reference initial soil moisture (*B100*) leads to roughly 10% higher precipitation values than in dry soil conditions. Microphysical perturbations (i.e., modified CCN concentrations and ν values) lead to a change in precipitation from −14% for small values (i.e., clean air with broad CDSD) to +10% for moderately large values ($\nu = 2$; CCN = 1700 cm^{-3}). Similar to the dry-bias experiments, the no-bias simulations mostly show a sawtooth-like increasing trend for CCN concentrations smaller than 3200 cm^{-3} and an interruption of the trend for the highest CCN concentration parameter (3200 cm^{-3}).

The effect of a further increase in initial soil moisture by 25% (i.e., from *B100* to *B125*) is less consistent. Relating the *B125* experiments to the reference simulation shows that the overall change in accumulated precipitation ranges only between −3% and +8%. However, a closer look comparing individual *B125* experiments sharing an identical microphysical setting reveals that only those experiments with a small to moderate CCN concentration (100 and 600 cm^{-3}) indicate an increase of 10–15% in precipitation relative to the respective experiment with reference initial soil moisture, whereas experiments with

higher CCN concentration show a decrease. This altered sensitivity of accumulated precipitation to the perturbations hints at a change in the evaporation regime, moving from a moisture-limited towards an energy-limited regime (Koster *et al.*, 2009).

In summary, the macro- and microphysical perturbations can alter accumulated precipitation by roughly between −20% and 10%. For most of the experiments, precipitation increases with increasing initial soil moisture, increasing shape parameter (ν; i.e., narrower CDSD), and increasing CCN concentration. This leads to the sawtooth-like shape of relative precipitation within each soil-moisture group in Figure 5a. On average, we find positive soil-moisture, CCN, and CDSD–precipitation couplings for small and moderate microphysical perturbations, that is, maritime to continental aerosol assumptions.

To elucidate the impact of the perturbations on the formation of precipitation, we now examine cloud clusters (rather than TQC) as a precursor of precipitation. Cloud clusters are defined as an area of connected grid cells with the liquid water path exceeding 50 $g \cdot m^{-2}$, similar to Barthlott and Hoose (2018). Based on this classification, Figure 5b depicts the total number of cloud clusters accumulated between 0900 and 2100 UTC for each experiment. Cloud clusters lasting longer than one output interval are only counted once in this 12-hr period.

In contrast to precipitation, the number of cloud clusters is almost constantly decreasing with increasing soil moisture, increasing CCN concentration, and increasing shape parameter, indicating a negative coupling. While there are up to 900 clusters counted in the experiment with dry soil conditions and clean air with larger cloud droplets, there are only about 500 clouds for wet and polluted conditions. At first sight, this is partly contradictory to the behaviour of accumulated precipitation. Two different hypotheses are examined in the following: moister initial soil conditions lead firstly to more efficient precipitating cloud clusters, or secondly to clouds that form larger clusters, which persist longer.

Figure 6 shows (a–c) a time series of the number of cloud clusters, as well as (d–f) the average size of cloud clusters, coloured according to (a,d) initial soil moisture, (b,e) CCN concentration, and (e,f) the shape parameter. Similar to the temporally aggregated number of cloud clusters (Figure 5b), the time series of cloud amount shows a clear sensitivity to the initial soil moisture (Figure 6a). Before 1600 UTC, the three groups are clearly distinct from each other. Dry initial soil conditions reach an early maximum at about 1300 UTC, with a cloud amount between 270 and 300 clusters. The maximum number of cloud clusters for moist initial soil conditions is reached about 1.5 hr later and only amounts to 200–240 cloud clusters, whereas for experiments with unperturbed soil

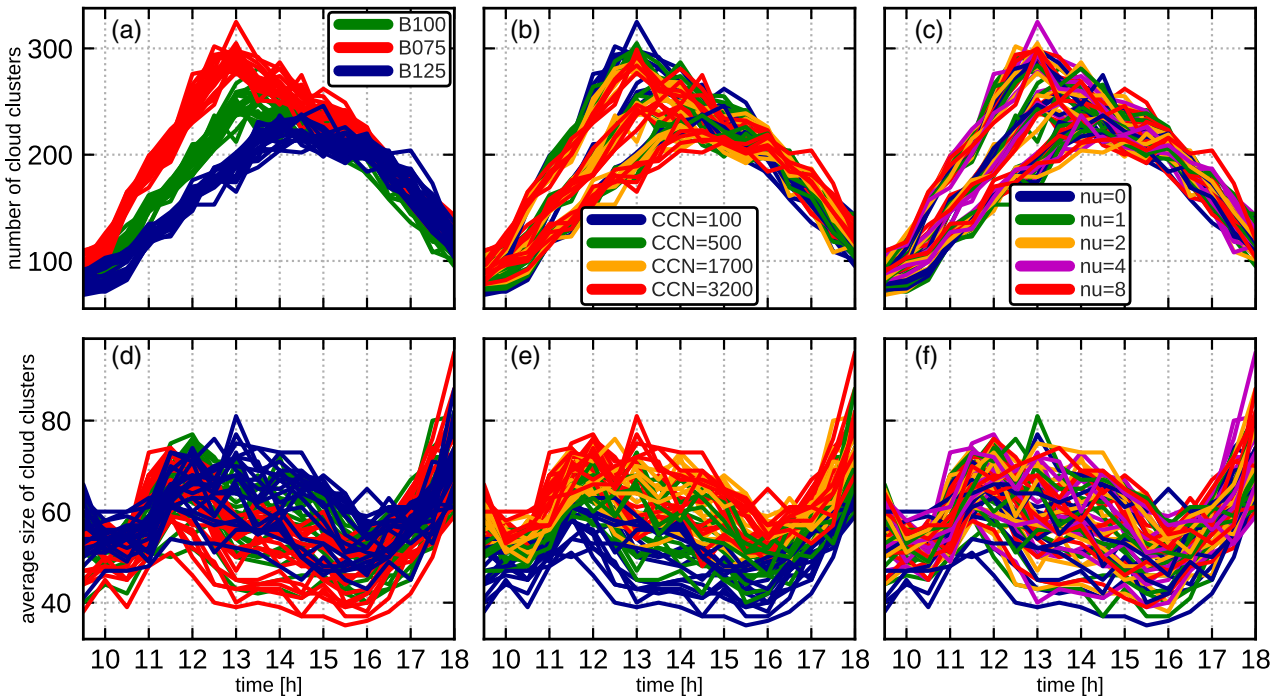

FIGURE 6 Time series of the convective period from 0900–1800 UTC of (a–c, upper row) the domain-averaged number of cloud clusters and (d–f, lower row)average cloud cluster size. Each row shows the same data, but coloured according to (a,d) the initial soil moisture, (b,e) concentration of cloud condensation nuclei, or (c,f) shape parameter [Colour figure can be viewed at wileyonlinelibrary.com]

conditions the numbers lie in between. The envelopes of the three distinct line groups (explaining the range of variability within one soil-moisture perturbation) remain similar throughout the period. Furthermore, the number of cloud clusters is secondarily sensitive to the CCN concentration (Figure 6b). Looking at the maxima of the three line groups, high CCN concentrations (red) tend to be at the lower end, describing a reduction in cloud clusters, whereas low CCN concentrations (blue) are mostly at the upper bound, indicating an increased number of cloud clusters. In contrast, there is no systematic response to the shape of the CDSD discernible (Figure 6c).

Complementary to the time series of the number of cloud clusters, the average cluster sizes are depicted in Figure 6d–f. The coupling between the perturbations and the size of the cloud clusters is inverse to that of the number of cloud clusters described above, although the sensitivity is less clear than for the cloud amount. Hence, the cloud cluster size of moist initial soil conditions is shifted towards the upper range of values, with average sizes of up to 80 grid cells. Dry initial soil conditions, instead, show the smallest cloud clusters, with a minimum size of about 40 grid cells. Those differences are discernible between 1200 and 1600 UTC, the time period with the maximum number of cloud clusters. Consequently, there is a negative soil-moisture–cloud-amount coupling and a positive soil-moisture–cloud-size coupling (Figure 6a,d). Finally, the coupling between CCN concentration and cloud size is positive (as for precipitation totals, but inverse to the cloud numbers), with the largest cluster sizes for high CCN concentrations (red; Figure 6e). Accordingly, low CCN concentrations (blue) result in smaller cluster sizes. Similar to the number of clouds, the sensitivity of the cloud size to CDSD is barely visible (Figure 6c,f).

In addition to the number and size of cloud clusters, the average lifetime of cloud clusters is positively correlated with soil moisture, CCN concentration, and CDSD, as suggested above. However, the variations are on average less than 30 min (Figure 5c). In conclusion, cloud clusters grow larger and persist longer but are fewer given moist soil conditions and high CCN concentrations. Vice versa, there are more, but smaller and short-lived cloud clusters present in dry soil and clean aerosol conditions, which ultimately lead to less precipitation (see Figures 5 and 6).

3.3 | Precipitation efficiency and microphysical process rates

To examine further the nonlinear increase in precipitation but quasilinear decrease in the number of cloud clusters (sawtooth-like increase versus rather constant decrease in Figure 5a,b, respectively) for moister soils and more polluted conditions, we apply the concept of precipitation efficiency (PE) to the various experiments. PE is defined as the ratio of hourly precipitation (P, $\mathrm{kg \cdot m^{-2} \cdot h^{-1}}$) to the sum of all processes generating condensates in the atmosphere (G):

$$PE = \frac{P}{G}. \tag{1}$$

The generation term G comprises the microphysical processes deposition, riming, autoconversion, and accretion. Other PE definitions, for example, by Khain (2009), use only condensation and ice deposition for condensate generation. In this study, however, we consider all microphysical processes leading to hydrometeor types forming surface precipitation (i.e., rain, ice, snow, graupel, and hail) and thereby neglect the condensation of cloud droplets. As melting and freezing is only a redistribution between precipitating particle classes, these processes are also not included.

The domain- and time-averaged value of PE is shown in Figure 5a for each experiment (black crosses). Comparing the three initial soil-moisture groups reveals that PE is barely sensitive to the soil-moisture content. Instead, PE exhibits a distinct sensitivity to the microphysical parameter setting, as it increases with increasing CCN concentration and increasing shape parameter ν. Independent of the initial soil moisture, PE deviations from the respective reference run range from about −18% for clean air and broad CDSD to about +20% for polluted conditions with a narrower CDSD. The sensitivity of PE to the shape parameter resembles the sawtooth-like increase in surface precipitation (orange circles in Figure 5a). This is most evident for the drier *B075* and reference *B100* experiments.

Interestingly, PE resembles the largely systematic response of surface precipitation to many combined microphysical perturbations. However, PE keeps increasing in more polluted conditions and with narrower CDSD (larger values of microphysical parameters), while surface precipitation shows a decay. This hints at processes masking the systematic influence of microphysical perturbations on PE when focusing on surface precipitation.

Since PE comprises the ratio of precipitation rate and microphysical processes changing cloud condensate, we show vertical profiles of the various process rates and the ensuing condensates to shed light on important mechanisms. Figure 7 shows the time- and domain-averaged cloud and rain water, as well as various microphysical process rates included in PE, for the experiments without soil-moisture perturbations (*B100*). In maritime CCN conditions, we find the lowest amount of cloud water (QC), but the highest rain water (QR) content. An increase in CCN concentration leads systematically to less QR, but more QC caused by reduced autoconversion

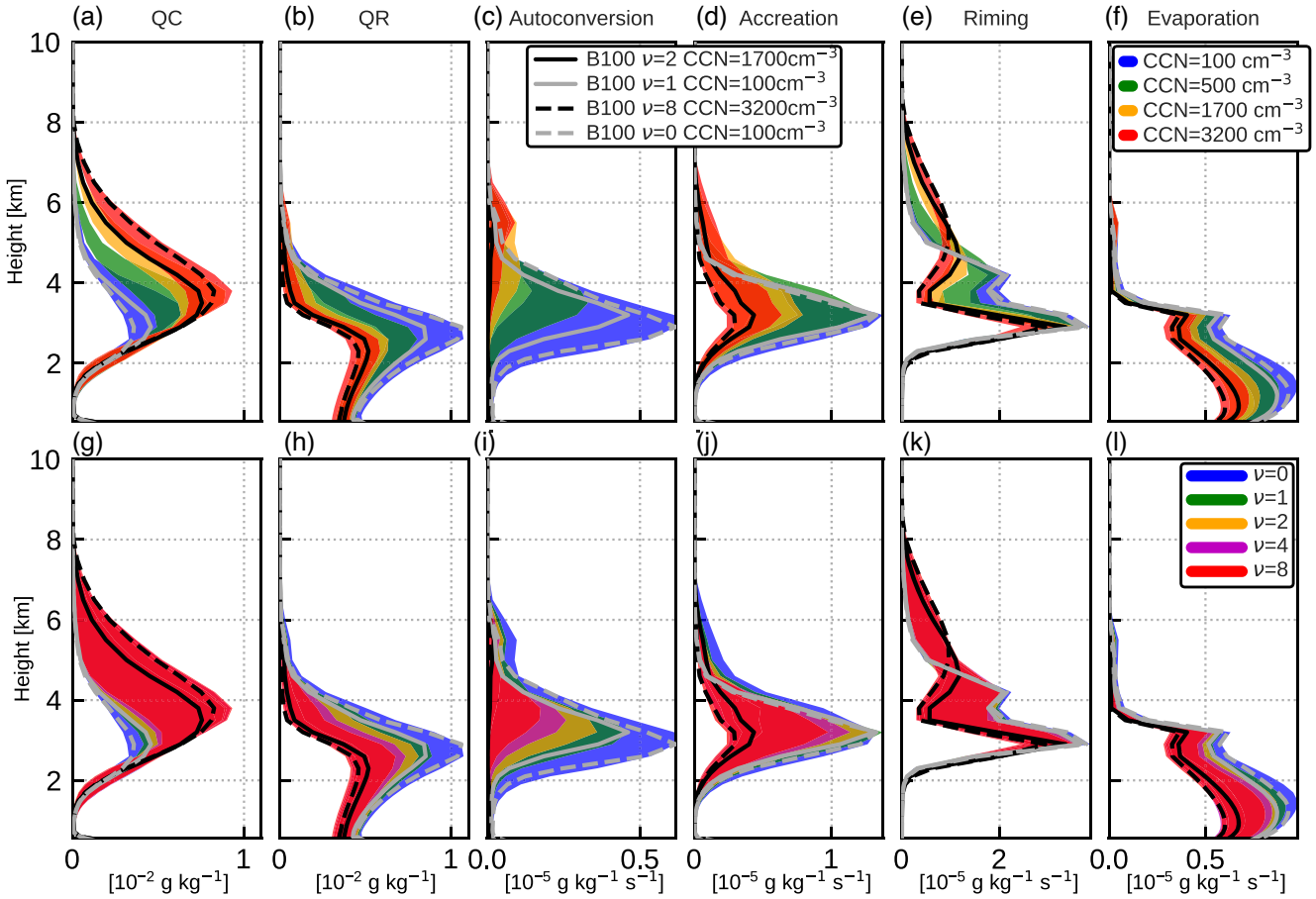

FIGURE 7 Envelopes of vertical profiles of spatially and temporally (09002100 UTC) averaged (a,g) cloud water (QC) and (b,h) rain water (QR), as well as, microphysical process rates for (c,i) autoconversion, (d,j) accretion, (e,k) riming, and (f,l) evaporation are shown. All experiments are considered in this figure. Both rows comprise the same data with different colouring. The first row (a–f) displays all experiments coloured according to their aerosol concentration (blue: CCN = 100 cm^{-3}; green: CCN = 500 cm^{-3}; yellow: CCN = 1700 cm^{-3}; red: CCN = 3200 cm^{-3}), whereas the second row (g–l) groups the experiments according to the shape parameter ν. Additionally, single profiles show the experiments (all *B100*) with the lowest ($\nu = 1$; CCN = 100 cm^{-3}, grey (blue in Figure 3)) and highest ($\nu = 2$; CCN = 1700 cm^{-3}, black (red in Figure 3)) accumulated precipitation. Maximum/minimum microphysical PE are achieved by choosing $\nu = 8$; CCN = 3200 cm^{-3} (black, dashed)/$\nu = 0$; CCN = 100 cm^{-3} (grey, dashed) profiles [Colour figure can be viewed at wileyonlinelibrary.com]

(Figure 7c) and accretion (Figure 7d) rates pointing towards a suppression of the warm-rain process, as was already found for simulations of a mesoscale convective system by Barthlott *et al.* (2017). This is in agreement with the general assumption that additional aerosols acting as CCN result in more numerous and smaller cloud droplets and therefore suppress the onset of precipitation in warm clouds as a result of the less efficient collision–coalescence process. Riming decreases systematically with increasing CCN concentration at altitudes between 3 and 5 km.

Evaporation is strongest for clean conditions and peaks below 2-km height (Figure 7f), thus contributing to the strong reduction of QR below 3 km. The strengthened evaporation is caused by the increased number of smaller rain droplets that form under clean conditions, as was shown by Altaratz *et al.* (2008). To test this, we computed raindrop size distributions at various levels for several integration times (not shown), and we find that the distributions shift to populations of raindrops that are fewer in number but larger in size in more polluted conditions. Due to a smaller surface area relative to their volume, larger raindrops do not evaporate as quickly in clean conditions (e.g., Barthlott *et al.*, 2017). However, they show the highest QR values, despite the low QC content and maximal evaporation rates for clean conditions.

The sensitivity of microphysical processes to the shape parameter is similarly systematic, albeit less pronounced, and has the same coupling sign as for the CCN concentration. Similar to the CCN sensitivity, QC (Figure 7g) and QR (Figure 7h) show a contrasting response, with a positive coupling of QC and negative coupling of QR to an increased shape parameter. For instance, autoconversion and accretion are negatively correlated with the shape parameter, leading to maximum values for small

shape parameters (Figure 7i,j). The narrowing of the CDSD with larger shape parameters reduces the efficiency of the collision–coalescence process and therefore has a similar effect on QC and QR than the increase in CCN concentrations. In particular, we find a significant reduction of autoconversion of roughly −83% for the highest shape parameter of $\nu = 8$, compared with its reference value of 0 (considering reference CCN). The fact that precipitation mostly still increases with larger shape parameters (see Figure 5) indicates that cold rain processes dominate and play a larger role for precipitation totals for these conditions.

The dominance of cold-rain processes is also supported by Figure 8, showing the ratio of the aggregated vapour deposition and riming to the sum of accretion and autoconversion. Values greater than 1 imply a larger contribution of cold-rain formation processes. For domain-averaged precipitation rates above 0.05 mm $(30\,\text{min})^{-1}$, the ratio is larger than 2, or even larger for precipitation above 0.20 mm $(30\,\text{min})^{-1}$. This generally hints at a predominance of cold-rain processes. Looking more closely, increasing microphysical parameters even increase the dominance of cold-rain processes. While the ratio of a small CCN concentration (Figure 8a) and a small shape parameter (Figure 8b), respectively, shunts at the lower end, large microphysical parameters lead to large ratios. While the ratio of a small CCN concentration (Figure 8a) or a small shape parameter (Figure 8b) ranks at the lower end, large microphysical parameters lead to large ratios. Consequently, increasing microphysical parameters actually increase the dominance of cold-rain processes. In particular, the suppressed collision–coalescence process leads to more supercooled liquid droplets above freezing level (Figure 7a,g), which can also foster cold-rain formation by higher latent heat release.

The microphysical process rates themselves behave quasilinearly and show extreme values for extreme perturbations. The lowest process rates are found for the smallest values of the microphysics parameters ($\nu = 0$, CCN = 100 cm^{-3}, i.e., low aerosol content and broad CDSD; grey dashed), leading to a reduction of PE by −19% (*B075*) or −16% (*B100*) relative to the reference

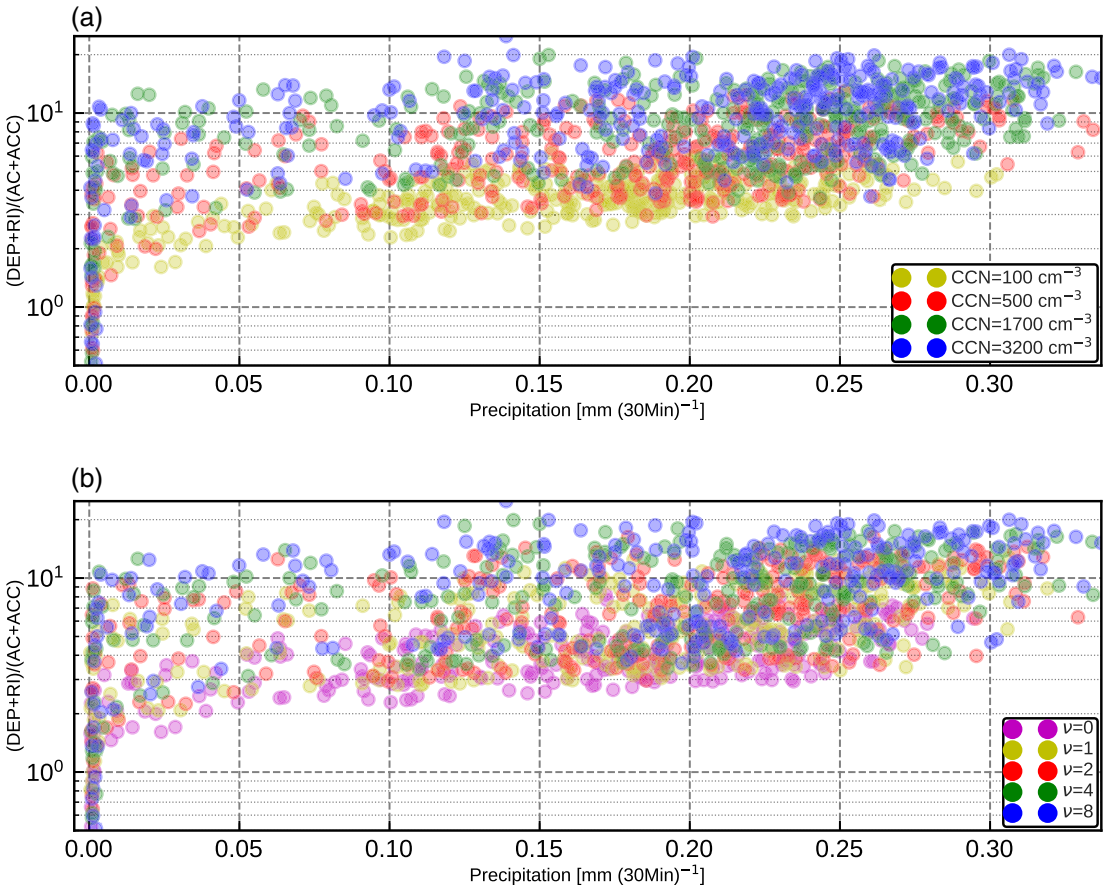

FIGURE 8 Ratio between cold-rain (deposition (DEP) and riming (RI)) and warm-rain (autoconversion (AC) and accretion (ACC)) formation processes relative to domain-averaged precipitation. Both panels show all experiments and a 30-min output interval, whereas data are coloured according to CCN concentration in (a) and according to the shape parameter in (b) [Colour figure can be viewed at wileyonlinelibrary.com]

simulation, depending on the initial soil moisture. Conversely, the highest process rates are encountered when choosing maximal values of microphysics parameters ($\nu = 8$, CCN $= 3200\,\mathrm{cm}^{-3}$, i.e., high aerosol load and narrow CDSD; black dashed), increasing PE by +20% (*B100*, *B125*). In agreement with the process rates, evaporation also increases, reducing the large differences in QR. However, these extreme microphysical parameter settings do not lead to the highest or lowest precipitation amounts, respectively. In fact, the most intense (Figure 3; red) and weakest surface precipitation (Figure 3; blue) are found in experiments with other (not extreme) microphysical parameter settings, denoted in Figure 7 by the grey solid line (max: $\nu = 2$, CCN $= 1700\,\mathrm{cm}^{-3}$) and black solid line (min: $\nu = 1$, CCN $= 100\,\mathrm{cm}^{-3}$). Note that these two profiles only consider *B100* experiments, to increase readability. The largest discrepancies between the maximization of process rates (grey dashed) and the minimization of surface precipitation (grey solid) is evident for QR (Figure 7b,h), autoconversion (Figure 7c,i), and evaporation (Figure 7f,l). Including the effect of initial soil moisture even increases the differences in evaporation (not shown). Evaporation, the most prominent process removing QR, increases with decreasing microphysical parameters, removes the large differences in QR, and reduces precipitation, overruling the increase in autoconversion. Furthermore, the distinct negative correlation between evaporation and the shape of CDSD maintains a sawtooth-like behaviour of precipitation.

4 | SUMMARY AND CONCLUSIONS

For the first time, the combined influence of soil-moisture bias and two microphysical uncertainties (i.e., the shape parameter of the cloud droplet size distribution (CDSD) and the amount of CCN) in real-case numerical simulations of convective clouds and precipitation is explored. Using the same modelling framework as in previous work (e.g., Barthlott and Hoose, 2018; Baur *et al.*, 2018; Keil *et al.*, 2019), namely the COSMO model at convection-permitting resolution driven with the same source of analysis data as initial and hourly lateral boundary conditions, allows for the identification of uncertainty resulting from combined land-surface and microphysical perturbations. Since several studies suggest a stronger fingerprint during weakly forced atmospheric conditions, we constrain the numerical experimentation in this pilot study and apply the concept of combined sensitivities to a single day. The case of 6 June, 2016 has been selected as a typical atmospheric scenario governed by weak synoptic control. This day is part of a well-studied 10-day period characterized by frequent heavy precipitation events in late May–early June 2016 and serves as a prototype case for exploration of the collective impact. For that purpose, a series of COSMO simulations with three different initial soil-moisture settings, four different spatially homogeneous CCN concentrations, and five different shape parameters (ν) of CDSD summing up to 60 experiments was performed.

As already shown in earlier studies (e.g., Baur *et al.*, 2018, and references therein), domain-averaged precipitation generally increases with initial soil moisture. The increase in precipitation, however, is limited, as the evaporative regime transits from a moisture-limited (*B075*, *B100*) to an energy-limited regime (B125). Further moistening of the soil thus does not increase moisture supply to the atmosphere and hence does not increase precipitation further. Still, initial soil moisture influences the triggering of convection, with dry conditions accelerating and moist conditions decelerating its onset within the first hours. Our results thus show a negative soil-moisture–precipitation coupling during the initiation phase and a positive coupling afterwards.

In contrast to the behaviour of surface precipitation, the number of cloud clusters decreases continuously with increasing initial soil moisture, narrowing CDSD, and increasing CCN concentration. This is counterintuitive, as clouds are considered to be a precursor to precipitation. An increase in average cloud size and a slightly longer lifetime counteracts the decreasing number, while not being as systematic (e.g., Figure 6a,d). More precisely, this approach does not explain the distinct sensitivity of precipitation to CDSD. That hints at other processes influencing the efficiency of clouds in forming precipitation in light of the perturbed microphysical parameters.

The precipitation efficiency PE, the ratio of hourly precipitation to the sum of all processes producing or amplifying condensates, parallels the increase in precipitation totals, in contrast to the number of clouds. PE is scarcely influenced by initial soil moisture, but is sensitive to microphysical parameters, unlike precipitation. We find that the formation of raindrops and their evaporation are both negatively coupled with the microphysical parameter settings. However, increased evaporation counteracts the increased rain water content (QR) and masks the effect of the microphysical perturbations on surface precipitation.

For clean air with low aerosol concentrations, typical for maritime air, the PE is lowest and the process rates are largest. In contrast, PE is highest (synonymous with the smallest process rates) in continental polluted conditions (high CCN) and with the narrowest CDSD. Relative to the reference simulation, PE varies in a range of about ±20%. Consequently, extreme microphysical settings cause

extreme values in PE. However, the extreme microphysical settings do not result in extreme precipitation values. Small, not minimal values of the microphysical parameters ($\nu = 1$; CCN $= 100\,\mathrm{cm}^{-3}$) reduce precipitation by about 14%, whereas moderately large values ($\nu = 2$; CCN $= 1700\,\mathrm{cm}^{-3}$) increase rainfall by about 10%. Since precipitation efficiency does not differ between moderate and extreme perturbations, a process depleting raindrops must be acting in the atmosphere.

Adding initial soil-moisture perturbations shows that a reduction in surface evaporation by reducing initial soil moisture reduces surface precipitation further (−23% compared with the reference), while PE remains similar. Due to the reduced moisture input from the surface, minimal precipitation is indeed achieved with the smallest values in the microphysics (i.e., $\nu = 0$; CCN $= 100\,\mathrm{cm}^{-3}$). Alternatively, increasing initial soil moisture does not increase accumulated precipitation further, due to the change in evaporative regime.

Concluding, minimizing/maximizing microphysical process rates in the vertical column does not minimize/-maximize surface precipitation. There are compensating effects, such as evaporation, masking the sensitivity of the perturbations to surface precipitation. In other words, precipitation formation might be more efficient, but surface precipitation does not change, due to relatively increased evaporation. While the efficiency of forming precipitation is almost unrelated to soil moisture, evaporation is largely dependent on moisture input from the surface. These compensating effects explain why the number of cloud clusters, their sizes, and the surface precipitation do not change consistently or linearly.

Besides that, microphysical processes also influence the formation process of precipitation strongly. Similar to the synoptically weakly forced cases in Barthlott and Hoose (2018), cold-rain processes predominate, with ratios of the same order of magnitude (see Figure 8). Furthermore, the evaluations shown here imply an enhanced importance of cold-rain processes with increasing microphysical parameter settings. While small parameters (i.e., small shape parameter or small CCN concentration) tend to be at the lower end of the ratios, the largest ratios occur for large microphysical parameters. Microphysical parameters thus shift the rain formation more towards cold-rain processes.

This work represents a pilot study covering a well-studied, characteristic weakly forced convective summer day in the midlatitudes. We believe that this study provides a first, albeit rough, but still trustworthy picture of the combined effect of soil moisture and microphysics perturbations on convective clouds and precipitation. Robust results, however, require a larger data base containing more case studies covering different synoptic situations (see, e.g., Barthlott *et al.*, 2022; Matsunobu *et al.*, 2022). Evaporation of raindrops is a key process that needs further investigation. Detailed knowledge of the existence of compensating or enhancing processes influencing the collective effect of macro- and microphysical perturbations on cloud formation and precipitation will play a key role in future convective-scale NWP systems. In future studies, such combined perturbations will be completed by taking into account the key sources of uncertainty in limited-area ensemble modelling at convective scales.

AUTHOR CONTRIBUTIONS

Florian Baur: Conceptualization; data curation; formal analysis; investigation; methodology; software; visualization; writing – original draft; writing – review and editing. **Christian Keil:** Conceptualization; formal analysis; investigation; methodology; supervision; writing – original draft; writing – review and editing. **Christian Barthlott:** Conceptualization; formal analysis; investigation; methodology; software; supervision; writing – review and editing.

ACKNOWLEDGEMENTS

Open Access funding was enabled and organized by Projekt DEAL.

ORCID

Florian Baur https://orcid.org/0000-0002-4330-0906
Christian Keil https://orcid.org/0000-0003-2736-4309

REFERENCES

Altaratz, O., Koren, I., Reisin, T., Kostinski, A., Feingold, G., Levin, Z. and Yin, Y. (2008) Aerosols' influence on the interplay between condensation, evaporation and rain in warm cumulus cloud. *Atmospheric Chemistry and Physics*, 8(1), 15–24. https://doi.org/10.5194/acp-8-15-2008.

Barthlott, C., Hauck, C., Schädler, G., Kalthoff, N. and Kottmeier, C. (2011) Soil moisture impacts on convective indices and precipitation over complex terrain. *Meteorologische Zeitschrift*, 20(2), 185–197. 10.1127/0941-2948/2011/0216.

Barthlott, C., Mühr, B. and Hoose, C. (2017) Sensitivity of the 2014 Pentecost storms over Germany to different model grids and microphysics schemes. *Quarterly Journal of the Royal Meteorological Society*, 143(704), 1485–1503. https://doi.org/10.1002/qj.3019.

Barthlott, C. and Hoose, C. (2018) Aerosol effects on clouds and precipitation over central Europe in different weather regimes. *Journal of the Atmospheric Sciences*, 75(12), 4247–4264. https://doi.org/10.1175/JAS-D-18-0110.1. ISSN 0022-4928.

Barthlott, C., Zarboo, A., Matsunobu, T. and Keil, C. (2022) Importance of aerosols and shape of the cloud droplet size distribution for convective clouds and precipitation. *Atmospheric Chemistry*

and Physics, 22(3), 2153–2172. https://doi.org/10.5194/acp-22-2153-2022. ISSN 1680-7316.

Baur, F., Keil, C. and Craig, G.C. (2018) Soil moisture–precipitation coupling over Central Europe: Interactions between surface anomalies at different scales and the dynamical implication. *Quarterly Journal of the Royal Meteorological Society*, 144(717), 2863–2875. https://doi.org/10.1002/qj.3415. ISSN 1477-870X.

Cioni, G. and Hohenegger, C. (2017) Effect of soil moisture on diurnal convection and precipitation in large-eddy simulations. *Journal of Hydrometeorology*, 18(7), 1885–1903. https://doi.org/10.1175/JHM-D-16-0241.1.

Fan, J., Wang, Y., Rosenfeld, D. and Liu, X. (2016) Review of aerosol–cloud interactions: mechanisms, significance, and challenges. *Journal of the Atmospheric Sciences*, 73(11), 4221–4252. https://doi.org/10.1175/JAS-D-16-0037.1. ISSN 0022-4928, 1520-0469.

Glassmeier, F. and Lohmann, U. (2018) Precipitation susceptibility and aerosol buffering of warm- and mixed-phase orographic clouds in idealized simulations. *Journal of the Atmospheric Sciences*, 75(4), 1173–1194. https://doi.org/10.1175/JAS-D-17-0254.1.

Grant, L.D. and van den Heever, S.C. (2015) Cold pool and precipitation responses to aerosol loading: Modulation by dry layers. *Journal of the Atmospheric Sciences*, 72(4), 1398–1408. https://doi.org/10.1175/JAS-D-14-0260.1.

Hauck, C., Barthlott, C., Krauss, L. and Kalthoff, N. (2011) Soil moisture variability and its influence on convective precipitation over complex terrain. *Quarterly Journal of the Royal Meteorological Society*, 137(S1), 42–56. https://doi.org/10.1002/qj.766. ISSN 1477-870X.

Hirt, M., Rasp, S., Blahak, U. and Craig, G.C. (2019) Stochastic parameterization of processes leading to convective initiation in kilometer-scale models. *Monthly Weather Review*, 147(11), 3917–3934. https://doi.org/10.1175/MWR-D-19-0060.1.

Hohenegger, C., Brockhaus, P., Bretherton, C.S. and Schär, C. (2009) The soil moisture precipitation feedback in simulations with explicit and parameterized convection. *Journal of Climate*, 22(19), 5003–5020. https://doi.org/10.1175/2009JCLI2604.1.

Igel, A.L. and van den Heever, S.C. (2017a) The importance of the shape of cloud droplet size distributions in shallow cumulus clouds. Part I: Bin microphysics simulations. *Journal of the Atmospheric Sciences*, 74(1), 249–258. https://doi.org/10.1175/JAS-D-15-0382.1.

Igel, A.L. and van den Heever, S.C. (2017b) The importance of the shape of cloud droplet size distributions in shallow cumulus clouds. Part II: Bulk microphysics simulations. *Journal of the Atmospheric Sciences*, 74(1), 259–273. https://doi.org/10.1175/JAS-D-15-0383.1.

Imamovic, A., Schlemmer, L. and Schär, C. (2017) Collective impacts of orography and soil moisture on the soil moisture–precipitation feedback. *Geophysical Research Letters*, 44(22), 11,682–11,691. https://doi.org/10.1002/2017GL075657. ISSN 1944-8007.

Keil, C., Baur, F., Bachmann, K., Rasp, S., Schneider, L. and Barthlott, C. (2019) Relative contribution of soil moisture, boundary-layer and microphysical perturbations on convective predictability in different weather regimes. *Quarterly Journal of the Royal Meteorological Society*, 145(724), 3102–3115. https://doi.org/10.1002/qj.3607. ISSN 0035-9009, 1477-870X.

Khain, A.P. (2009) Notes on state-of-the-art investigations of aerosol effects on precipitation: A critical review. *Environmental Research Letters*, 4(1), 015004. https://doi.org/10.1088/1748-9326/4/1/015004.

Kirshbaum, D.J., Adler, B., Kalthoff, N., Barthlott, C. and Serafin, S. (2018) Moist orographic convection: Physical mechanisms and links to surface-exchange processes. *Atmosphere*, 9(3), 80. https://doi.org/10.3390/atmos9030080.

Koster, R.D., Guo, Z., Yang, R., Dirmeyer, P.A., Mitchell, K. and Puma, M.J. (2009) On the nature of soil moisture in land surface models. *Journal of Climate*, 22(16), 4322–4335. https://doi.org/10.1175/2009JCLI2832.1. ISSN 0894-8755.

Matsunobu, T., Zarboo, A., Barthlott, C. and Keil, C. (2022) Impact of combined microphysical uncertainties on convective clouds and precipitation in ICON-D2-EPS forecasts during different synoptic control. *Weather and Climate Dynamics [preprint]*, 1–25. https://doi.org/10.5194/wcd-2022-17. Under review.

Morrison, H. and Grabowski, W.W. (2007) Comparison of bulk and bin warm-rain microphysics models using a kinematic framework. *Journal of the Atmospheric Sciences*, 64(8), 2839–2861. https://doi.org/10.1175/JAS3980.

Piper, D., Kunz, M., Ehmele, F., Mohr, S., Mühr, B., Kron, A. and Daniell, J. (2016) Exceptional sequence of severe thunderstorms and related flash floods in May and June 2016 in Germany – Part 1: Meteorological background. *Natural Hazards and Earth System Sciences*, 16(12), 2835–2850. https://doi.org/10.5194/nhess-16-2835-2016. ISSN 1684-9981.

Rasp, S., Selz, T. and Craig, G.C. (2018) Variability and clustering of midlatitude summertime convection: Testing the Craig and Cohen theory in a convection-permitting ensemble with stochastic boundary layer perturbations. *Journal of the Atmospheric Sciences*, 75(2), 691–706. https://doi.org/10.1175/JAS-D-17-0258.1. ISSN 0022-4928.

Schättler, U., Doms, G. and Schraff, C. (2018). Part VII: User's Guide. In:, *A description of the nonhydrostatic regional COSMO-model*, pp. 181. Offenbach am Main, Germany: Deutscher Wetterdienst.

Schneider, L., Barthlott, C., Hoose, C. and Barrett, A.I. (2019) Relative impact of aerosol, soil moisture, and orography perturbations on deep convection. *Atmospheric Chemistry and Physics*, 19(19), 12343–12359. https://doi.org/10.5194/acp-19-12343-2019. ISSN 1680-7316.

Segal, Y. and Khain, A. (2006) Dependence of droplet concentration on aerosol conditions in different cloud types: Application to droplet concentration parameterization of aerosol conditions. *Journal of Geophysical Research: Atmosphere*, 111(D15), D15204. https://doi.org/10.1029/2005JD006561. ISSN 2156-2202.

Seifert, A. and Beheng, K.D. (2006) A two-moment cloud microphysics parameterization for mixed-phase clouds. Part 1: Model description. *Meteorology and Atmospheric Physics*, 92(1–2), 45–66. https://doi.org/10.1007/s00703-005-0112-4. ISSN 0177-7971, 1436-5065.

Seifert, A., Köhler, C. and Beheng, K.D. (2012) Aerosol–cloud–precipitation effects over Germany as simulated by a convective-scale numerical weather prediction model. *Atmospheric Chemistry and Physics*, 12(2), 709–725. https://doi.org/10.5194/acp-12-709-2012. ISSN 1680-7316.

Seneviratne, S.I., Corti, T., Davin, E.L., Hirschi, M., Jaeger, E.B., Lehner, I., Orlowsky, B. and Teuling, A.J. (2010) Investigating soil moisture–climate interactions in a changing climate: A review. *Earth-Science Reviews*, 99(3), 125–161. https://doi.org/10.1016/j.earscirev.2010.02.004. ISSN 0012-8252.

Wellmann, C., Barrett, A.I., Johnson, J.S., Kunz, M., Vogel, B., Carslaw, K.S. and Hoose, C. (2020) Comparing the impact of environmental conditions and microphysics on the forecast uncertainty of deep convective clouds and hail. *Atmospheric Chemistry and Physics*, 20(4), 2201–2219. https://doi.org/10.5194/acp-20-2201-2020.

Zeng, Y., Janjić, T., de Lozar, A., Blahak, U., Reich, H., Keil, C. and Seifert, A. (2018) Representation of model error in convective-scale data assimilation: additive noise, relaxation methods, and combinations. *Journal of Advances in Modeling Earth System*, 10(11), 2889–2911. https://doi.org/10.1029/2018MS001375. ISSN 1942-2466.

How to cite this article: Baur, F., Keil, C. & Barthlott, C. (2022) Combined effects of soil moisture and microphysical perturbations on convective clouds and precipitation for a locally forced case over Central Europe. *Quarterly Journal of the Royal Meteorological Society*, 148(746), 2132–2146. Available from: https://doi.org/10.1002/qj.4295